

Mechanical sensors

Multi-Material Torque Sensor Embedding One-Shot 3D-Printed Deformable Capacitive Structures

Jose Eduardo Aguilar-Segovia^{1*}, Maxime Manzano^{1*}, Sylvain Guégan², Ronan Le Breton², Alice Farhi-Rivasseau³, Sylvain Lefebvre⁴, and Marie Babel^{1**}

¹Université Rennes, INSA Rennes, Inria, CNRS, IRISA—UMR 6074, F-35000 Rennes, France

²Université Rennes, INSA Rennes, LGCGM, F-35000 Rennes, France

³ENS Rennes, 35170 Bruz, France

⁴Université de Lorraine, CNRS, Inria, LORIA, F-54600 Nancy, France

*Student Member, IEEE

**Member, IEEE

Manuscript received 18 July 2024; accepted 2 August 2024. Date of publication 7 August 2024; date of current version 20 August 2024.

Abstract—Measuring interaction forces between robots and humans is a major challenge in physical human–robot interactions. Nowadays, conventional force/torque sensors suffer from bulkiness, high cost, and stiffness, which limit their use in soft robotics. Thus, we introduce a novel torque sensor manufactured with material extrusion technology. Our approach relies on capacitive structures, which are at the same time the deformable and sensing parts of the sensor, making it very compact. These structures are made in one single print, simplifying the manufacturing process compared to traditional torque sensors. The sensor characteristics can be modulated thanks to material extrusion technology. We conduct experiments in a dedicated test bench to characterize the proposed torque sensor. From the characterization results, we implement a torque estimator based on the deformation angle estimate calculated from capacitance changes. The proposed torque sensor is able to measure torques within a ± 2.5 N·m range with a maximum error of 6% up to a deformation angle velocity of $35^\circ/\text{s}$. It is also able to measure its deformation angle with a maximum error of 0.4° . The accuracy of our sensor makes it suitable to ensure fine control in physical human–robot interaction applications.

Index Terms—Mechanical sensors, capacitive sensor, multimaterial extrusion (MEX) technology, physical human–robot interaction (pHRI), soft torque sensor.

I. INTRODUCTION

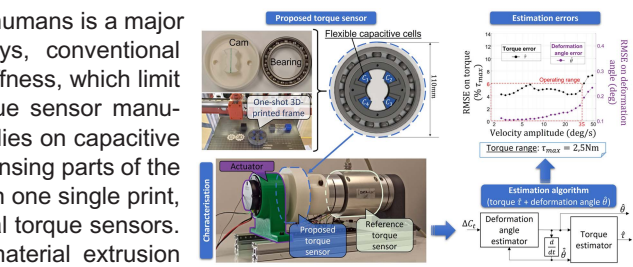
In the field of cobotics, assistive or social robotics, robots tend to reach a high level of cooperation and collaboration with the human agent in order to achieve joint actions. In this context, ensuring that the robot makes safe decisions requires to estimate the forces and torques exerted by the human [1]. Physical human–robot interaction (pHRI) is then essential in the control framework as it aims to provide a communication channel between the user and the robot [2]. Thus, force/torque sensors are an efficient way to interpret human intent.

Typically, force and/or torque sensors are made by strain-sensitive elements placed on a deformable part [3], which can be manufactured in different ways affecting the sensor stiffness and measurement range. The strain-sensitive elements can be resistive strain gauges, or capacitive or optoelectronic components [4]. However, these sensors are generally expensive, heavy, and bulky [5], whereas applications, such as exoskeletons, require the system to be lightweight and compliant. Using a torsion spring for the deformable part can reduce the weight and stiffness of the device [6], allowing to measure the deflection with conventional optoelectronic [7] or magnetic encoders [8]. However, these solutions suffer from complex design and poor modularity [9].

Corresponding authors: Jose Eduardo Aguilar-Segovia; Maxime Manzano (e-mail: jose-eduardo.aguilar-segovia@inria.fr; maxime.manzano@inria.fr).

Associate Editor: M. Bhattacharjee.

Digital Object Identifier 10.1109/LSENS.2024.3440195



3D-printing via material extrusion (MEX) opens possibilities for creating cost-effective and lightweight mechanical systems with sensing capabilities [10], [11]. Furthermore, 3D-printing allows the modulation of the device characteristics catering to different applications [12], making it an interesting alternative for creating torque sensors. In particular, Hendrich et al. [13] proposed to fabricate deformable parts using conventional 3D-printing materials, such as polylactic acid (PLA), and to measure their deflection with external sensors. While this approach benefits from reduced cost and weight, the deformation is due to complex printed shapes that limit the modularity of the sensor characteristics and its measurement range.

To use the full potential of 3D-printing, an innovative approach is to directly print the sensing parts during the fabrication process. This allows the sensor characteristics to be adjusted by locally modulating the electromechanical properties of the sensing parts. Stiglmeier et al. [9] identified that few torque sensors in the literature incorporate 3D-printed sensing parts [14], [15], [16]. Nevertheless, the dynamic effects of these types of sensors have yet to be studied.

In this letter, we then introduce a light-weight and cost-effective torque sensor made from MEX technology, suitable for robotic applications (see Fig. 1). It comprises three parts: a rigid frame with four capacitive structures, a cam, and a ball bearing. The capacitive structures are created in a single printing process, and serve as both the elastic and sensing parts, making it highly compact. The proposed sensor can measure both positive and negative torques. We conducted

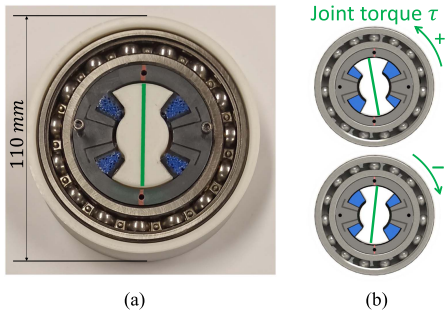


Fig. 1. (a) Picture of the proposed torque sensor. (b) Behavior under torque. For a given torque direction, two deformable capacitive structures are compressed, while the other ones are relaxed.

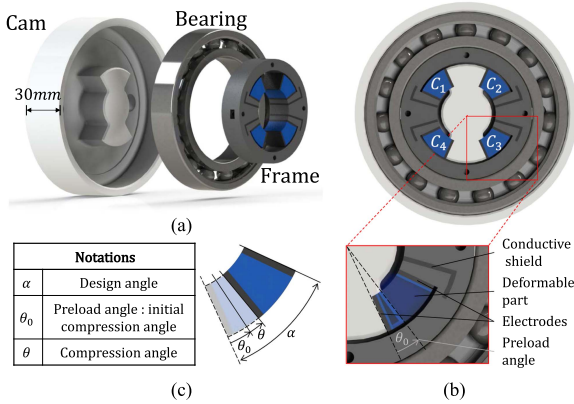


Fig. 2. Design of the proposed torque sensor. (a) General view showing the sensor parts. (b) Capacitive structure components. (c) Notations for the capacitive structures.

extensive experiments under quasi-static and dynamic conditions to characterize the sensor, and propose and evaluate a torque estimator.

II. METHODS

A. Sensor Design and Fabrication Process

The proposed torque sensor comprises three parts: a rigid frame with four deformable capacitive structures, a cam, and a ball bearing [see Fig. 2(a)]. The dimensions of the proposed torque sensor are 110 mm × 30 mm. The cam shape is designed to deform the capacitive structures when loaded by a torque. This torque is then estimated from the change of capacitance induced in these structures. To avoid backlash, the cam initially compresses the capacitive structures by a preload angle $\theta_0 = 6^\circ$, thus ensuring that they are always in compression. The ball bearing avoids friction while ensuring rotational guidance.

In this letter, we propose to fabricate our sensors through MEX technology. Our versatile design allows to modulate the characteristics of the capacitive structures by changing their infill pattern properties. Besides, the cam and frame can be made in a single print, which eases the fabrication process. Each of the four capacitive structures is made from two different thermoplastic polyurethane (TPU) materials, fused during the printing process: the electrodes are made of a flexible conductive material (Conductive Filaflex TPU, RECREUS), and the deformable part is made of a flexible nonconductive material (Filaflex 70 A, “Ultra-Soft,” RECREUS), as shown on Fig. 2(b). A conductive shield made from the same conductive material as the electrodes is added to prevent electromagnetic disturbances.

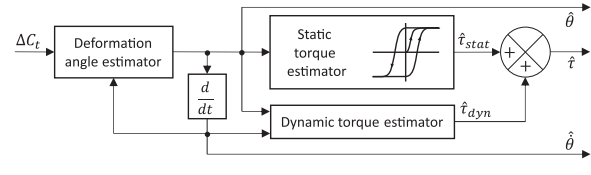


Fig. 3. Torque estimator pipeline. The deformation angle estimate ($\hat{\theta}$) is computed from the total capacitance change (ΔC_t) and used to derive the estimation of the angular velocity of deformation ($\hat{\theta}$). Both $\hat{\theta}$ and $\hat{\theta}$ are used to compute the torque estimate (\hat{t}) composed of a static and a dynamic component (respectively, \hat{t}_{stat} and \hat{t}_{dyn}).

The proposed sensor uses *square-grid infill pattern* for the deformable part of the capacitive structures, as it favors deformations in the plane normal to the joint axis [17]. It is fabricated with TPU and printed with a 50% density, while the cam and the rigid body of the frame are made in PLA. The frame integrating the capacitive structures is manufactured in a single print using a 3D-printer (ToolChanger, E3D Inc.) that operates up to four extruders. In our case, only three extrusion systems are used, each with a 0.4-mm diameter nozzle (Revo Hemera., E3D Inc.). The g-codes required to manufacture the frame and the cam are generated by IceSL software [18].

B. Working Principle

When a torque is applied, the cam rotates and compresses the capacitive structures by a deformation angle called θ , thus modifying their capacitance (C_i) [see Fig. 2(c)]. Compressing the capacitive structures reduces the interelectrode distance and increases their relative permittivity [19], leading to an increase in the capacitance value [20]. To estimate the torque, we then first compute the change ΔC_i of each capacitance as

$$\Delta C_i = C_i - C_{i\min} \quad (1)$$

with $C_{i\min}$ being the minimal value of C_i measured in the sensor working range. The total capacitance change is then computed as

$$\Delta C_t = \frac{1}{2}(\Delta C_1 - \Delta C_2 + \Delta C_3 - \Delta C_4). \quad (2)$$

As measuring the kinematics of the sensor is essential for safe and accurate control systems [21], the torque estimator module outputs the estimated torque value \hat{t} and estimated sensor kinematics, i.e., deformation angle $\hat{\theta}$ and angular velocity $\hat{\theta}$, from ΔC_t (see Fig. 3). Since TPU is considered a hyperviscoelastic material [22], the torque estimator relies on two main material properties: the “static torque estimator” includes a stress-strain hysteresis model, and the “dynamic torque estimator” compensates for the viscosity effect.

III. EXPERIMENTAL CHARACTERIZATION

A. Experimental Setup

The proposed torque sensor was characterized in a test bench composed of a brushless direct current (BLDC) motor (RMD X6S2, MyActuator) embedding an encoder for angle measurement and able to deliver up to ± 18 N·m torques, and an external torque sensor used as reference (DATAFLEX 22/20, KTR) able to measure up to ± 20 N·m torques with 1% measurement precision (see Fig. 4). A capacitance-to-digital converter (FCD1004, ProtoCentral) and a microcontroller are used to measure the capacitances. The measurement records and actuator commands run at 30 Hz.

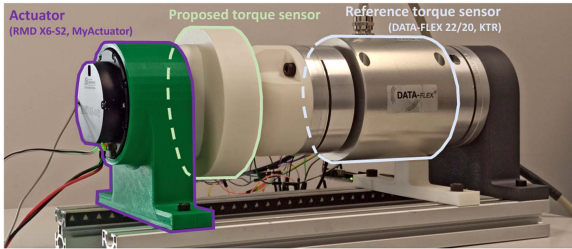


Fig. 4. Experimental setup. A BLDC motor actuates the proposed torque sensor while measuring the deformation angle θ . An external torque sensor measures the reference torque τ .

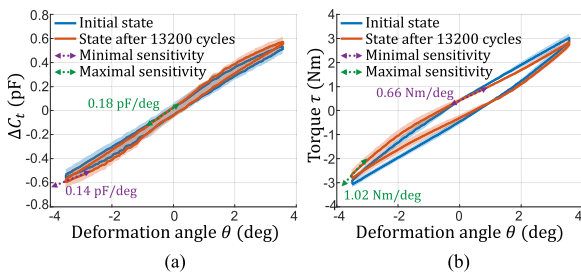


Fig. 5. Durability and repeatability results. Plots show the mean \pm standard deviation of (a) capacitance and (b) torque characteristics between the five printed sensors initially and after the durability trial. Extreme sensitivities within the measurement range are also indicated.

B. Characterization Process and Results

To measure the characteristics of the torque sensor, the actuator is controlled to follow angular sine waves of maximum 4° amplitude at different frequencies. The experimental setup allows for the generation of sine waves with frequencies up to 2 Hz, which corresponds to $\dot{\theta} = 50^\circ/\text{s}$ peak velocity.

To evaluate repeatability and durability, five sensors are manufactured with the same process and examined just after printing as well as after experiencing 13200 cycles (i.e., 11 h) of 4° amplitude (see Fig. 5). The results show that the sensors are slightly softer than they were initially, but they remain functional after the durability test. Furthermore, they show consistency across prints, as the maximum standard deviation within the measurement range is 0.05 pF for ΔC_t and 0.23 N·m for τ after the durability test. The minimal and maximal sensitivities for the deformation angle with respect to ΔC_t are 0.14 and 0.18 pF/ $^\circ$, respectively [see Fig 5(a)]. The minimal and maximal sensitivities for the deformation angle with respect to τ are 0.66 and 1.02 N·m/ $^\circ$, respectively [see Fig 5(b)].

To measure the sensor characteristics, a new sensor is manufactured and subjected to 1500 cycles to exceed its softening period, thereby stabilizing its mechanical properties. Then, the electromechanical characteristics of the torque sensor are measured at different deformation angle frequencies and amplitudes. For each frequency, 20 periods are performed. In the following, “quasi-static” and “dynamic” trials are considered. Quasi-static trials are performed at 0.1 Hz corresponding to $\dot{\theta} = 3^\circ/\text{s}$ where dynamic effects were negligible, and at amplitudes between 0.5° and 4° . The torque is called τ_{stat} in quasi-static. The dynamic characterization uses angular sine waves of 4° amplitude (i.e., its operating range) at different frequencies.

The results are shown in Fig. 6. Considering the quasi-static relationship between capacitance change (ΔC_t) and deformation angle θ , although we observe a disparity between the four capacitive structures, the total capacitance change ΔC_t is always almost linear with θ .

TABLE 1. Identified Estimator Parameter Values

$a(\text{pF}^{-1})$	$b(^{\circ})$	$c(\text{s})$	$m(\text{N}\cdot\text{m}^{-2}\text{s})$	$p(\text{N}\cdot\text{m}^{-1}\text{s})$
5.64	-0.27	0.015	0.001	0.02

Furthermore, a hysteresis effect is observed on the capacitance change-angle characteristic in quasi-static conditions [see Fig. 6(a)]. This hysteresis increases substantially with $\dot{\theta}$ [see Fig. 6(c)]. In addition, the torque–angle characteristic is quasi-linear, allowing to measure torques up to $\pm \tau_{\text{max}} = 2.5 \text{ N}\cdot\text{m}$. However, we observe a significant hysteresis effect even in quasi-static trials [see Fig. 6(b)] due to TPU mechanical behavior [22]. Because of viscosity, increasing $\dot{\theta}$ lowers the ascending branch and raises the descending one of the torque–angle hysteresis, reducing the distance between the branches until $\dot{\theta} \approx 17^\circ/\text{s}$, where both ascending and descending branches superimpose [see Fig. 6(d)]. Then, increasing $\dot{\theta}$ leads to an increase in the torque–angle hysteresis effect. Hence, in the following, we propose to define a torque estimator relying on kinematics estimation.

IV. TORQUE ESTIMATOR

Our proposed torque estimator runs in real time. In the first step, the total capacitance change ΔC_t (2) is used to estimate the deformation angle θ (see Fig. 3). It is defined as

$$\hat{\theta} = a\Delta C_t + b + c\hat{\theta} \quad (3)$$

with a , b , and c being constants. The term $c\hat{\theta}$ leads to an increase in the hysteresis effect, while the term $a\Delta C_t + b$ fits the quasi-static capacitance-angle characteristic [see Fig. 6(a)]. Then, the torque estimate $\hat{\tau}$ is computed from $\hat{\theta}$ and $\hat{\theta}$, with a static ($\hat{\tau}_{\text{stat}}$) and a dynamic ($\hat{\tau}_{\text{dyn}}$) components, inspired from Chiaradia et al. [23]. The first one determines $\hat{\tau}_{\text{stat}}$ by implementing a hysteresis-following algorithm of the literature [24] to follow the static torque–angle hysteresis. This algorithm uses two functions that fit either the ascending or descending branches. Then, the two functions are shifted to follow minor loops. The second component estimates $\hat{\tau}_{\text{dyn}}$ due to viscosity as

$$\hat{\tau}_{\text{dyn}} = m\hat{\theta}|\hat{\theta}| - p\hat{\theta} \quad (4)$$

with two constants m and p . The first term $m\hat{\theta}|\hat{\theta}|$ compensates for the stiffening effect due to viscosity [22], while the second one $-p\hat{\theta}$ makes ascending branches lowering and descending ones raising. The estimator parameters are derived from characterization curves and are given in Table 1.

V. RESULTS AND DISCUSSION

To illustrate the potential of our torque estimator, we evaluate its performance in the same scenario as for characterization (see Section III). The results demonstrate that our estimator accurately follows the dynamic behavior of the torque sensor (see Fig. 7). Notably, the global error remains below 6% of maximal torque τ_{max} within a range of 0–35°/s velocity amplitude. Besides, the deformation angle estimation error remains below 0.4° in this velocity range. In addition, as velocity increases, the relative error observed on $\hat{\tau}$ is significantly lower than the one observed on $\hat{\tau}_{\text{stat}}$, thus demonstrating the relevance of velocity compensation in torque estimation. The same phenomenon is observed in the deformation angle estimation.

Our proposed sensor has an extensive measurement range compared to 3D-printed torque sensors of the literature [9]. This range could be enlarged by increasing the density of the deformable part or using

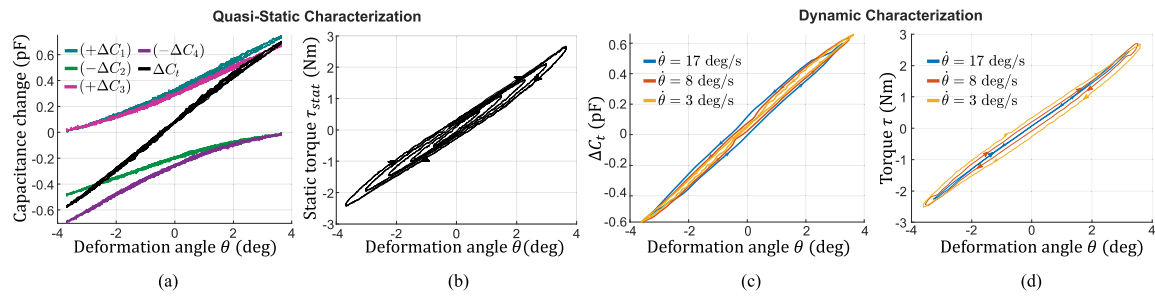


Fig. 6. Torque sensor characterization. Relationship between (a) deformation angle and capacitance change or (b) torque in quasi-static conditions for different angle amplitudes. (c) and (d) Dependence of these relationships with the angular deformation velocity $\dot{\theta}$.

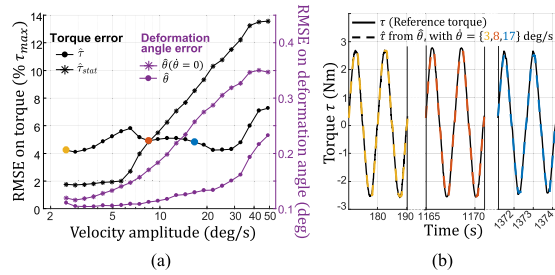


Fig. 7. Torque estimator assessment. (a) Root mean square error (RMSE) on τ and θ with different estimators, considering or not the dynamic part of the torque estimate ($\hat{\tau}$ and $\hat{\tau}_{\text{stat}}$, respectively). Deformation angles ($\hat{\theta}$) are estimated considering or not the effect of velocity change. (b) Torque estimator temporal behavior at three different velocities, emphasized with colored dots on the left plot.

a stiffer material. This highlights the versatility of our method for designing customizable torque sensors. Moreover, to the best of the authors' knowledge, measurement error in dynamic conditions is rarely evaluated in the literature. Chiaradia et al. [23] proposed a similar design and reached a similar error. However, their sensor is not fabricated in a single manufacturing process.

Future investigations will focus on improving the torque estimator by considering stress relaxation, studying the sensor behavior at higher frequencies, and increasing the sensor measurement range.

VI. CONCLUSION

In this letter, we present an innovative and lightweight torque sensor relying on deformable capacitive structures made in a single print. We extensively evaluate our sensor through experiments on a dedicated test bench. From characterization results, deformation angle and torque estimators are proposed. Results show that the proposed torque sensor is efficient to measure both torque and deformation angle, which makes it promising to be implemented in pHRI systems. The manufacturing process enables the easy modulation of the sensor characteristics. Our approach lays the groundwork for the extensive implementation of 3D-printed torque sensors in robotic systems. Future works will optimize the design and estimation algorithm of the proposed torque sensor and implement it in pHRI systems.

ACKNOWLEDGMENT

This work was supported by the Inria Defi under Project "DORNELL."

REFERENCES

- [1] D. P. Losey, C. G. McDonald, E. Battaglia, and M. K. O'Malley, "A review of intent detection, arbitration, and communication aspects of shared control for physical human–robot interaction," *Appl. Mech. Rev.*, vol. 70, Feb. 2018, Art. no. 010804.
- [2] H. J. Qi and M. C. Boyce, "Stress-strain behavior of thermoplastic polyurethanes," *Mech. Mater.*, vol. 37, no. 8, pp. 817–839, Aug. 2005.
- [3] D. Chiaradia, L. Tiseni, and A. Frisoli, "Compact series visco-elastic joint (SVEJ) for smooth torque control," *IEEE Trans. Haptics*, vol. 13, no. 1, pp. 226–232, Jan.–Mar. 2020.
- [4] A. Badel, J. Qiu, and T. Nakano, "A new simple asymmetric hysteresis operator and its application to inverse control of piezoelectric actuators," *IEEE Trans. Ultrasonics, Ferroelectrics, Freq. Control*, vol. 55, no. 5, pp. 1086–1094, May 2008.
- [5] H. Lee, S. J. Kim, H. Chang, and J. Kim, "Development of a compact optical torque sensor with decoupling axial-interference effects for pHRI," *Mechatronics*, vol. 52, pp. 90–101, Jun. 2018.
- [6] O. S. Al-Dahiere, R. A. R. Ghazilla, M. O. Tokhi, H. J. Yap, and M. Gul, "Design and characterization of a low-cost and efficient torsional spring for ES-RSEA," *Sensors (Basel)*, vol. 23, no. 7, Apr. 2023, Art. no. 3705.
- [7] W. M. dos Santos, G. A. P. Caurin, and A. A. G. Siqueira, "Design and control of an active knee orthosis driven by a rotary series elastic actuator," *Control Eng. Pract.*, vol. 58, pp. 307–318, Jan. 2017.
- [8] H.-T. Seo, J.-I. Park, and J. Park, "A compact series elastic element using a rubber compression mechanism," *Rev. Sci. Instruments*, vol. 92, no. 6, Jun. 2021, Art. no. 065004.
- [9] L. Stiglmeier, T. M. Wendt, and S. J. Rupitsch, "3-D-printed torque sensors: A review," *IEEE Sensors J.*, vol. 24, no. 12, pp. 18740–18761, 2024.
- [10] R. Chirila, O. Ozikoko, P. G. Schyns, and R. Dahiyat, "Multidirectional strain sensor using multimaterial 3D printing," in *Proc IEEE Int. Conf. Flexible Printable Sensors Syst.*, Jul. 2022, pp. 1–4.
- [11] M. Alalawi et al., "MechSense: A design and fabrication pipeline for integrating rotary encoders into 3D printed mechanisms," in *Proc. 2023 CHI Conf. Hum. Factors Comput. Syst.*, Apr. 2023, pp. 1–14.
- [12] M. Lalegani Dezaki, M. K. A. Mohd Ariffin, and S. Hatami, "An overview of fused deposition modelling (FDM): Research, development and process optimisation," *Rapid Prototyping J.*, vol. 27, no. 3, pp. 562–582, Jan. 2021.
- [13] N. Hendrich, F. Wasserfall, and J. Zhang, "3D printed low-cost force-torque sensors," *IEEE Access*, vol. 8, pp. 140569–140585, 2020.
- [14] M. Li, M. Assadian, M. Ramezani, and K. C. Aw, "Printed soft angular/torque sensors using carbon black-silicone composite," *Sensor Rev.*, vol. 39, no. 4, pp. 598–603, 2019.
- [15] G. D. Liu, C. H. Wang, Z. L. Jia, and K. X. Wang, "An integrative 3D printing method for rapid additive manufacturing of a capacitive force sensor," *J. Micromech. Microeng.*, vol. 31, no. 6, Jun. 2021, Art. no. 065005.
- [16] N. Soto, J. Garcia, and B. Newell, "Development of torque sensors using additive manufacturing," in *Smart Materials, Adaptive Structures and Intelligent Systems*, vol. 85499. New York, NY, USA: American Soc. Mechanical Eng., 2021.
- [17] M. T. Birosz, D. Ledenyak, and M. Ando, "Effect of FDM infill patterns on mechanical properties," *Polym. Testing*, vol. 113, 2022, Art. no. 107654.
- [18] "IceSL: A slicer and modeler," 2013. [Online]. Available: <https://icesl.loria.fr>
- [19] G. Stano, S. M. A. I. Ovy, J. R. Edwards, M. Cianchetti, G. Percoco, and Y. Tadesse, "One-shot additive manufacturing of robotic finger with embedded sensing and actuation," *Int J. Adv. Manuf. Technol.*, vol. 124, no. 1, pp. 467–485, Jan. 2023.
- [20] J. M. B. Barrachina, C. S. Cañas Peñuelas, and S. Catalán Izquierdo, "Capacitance evaluation on non-parallel thick-plate capacitors by means of finite element analysis," *J. Energy Power Eng.*, vol. 5, no. 4, pp. 373–378, 2011.
- [21] J. Vantilt et al., "Model-based control for exoskeletons with series elastic actuators evaluated on sit-to-stand movements," *J. NeuroEngineering Rehabil.*, vol. 16, no. 1, pp. 1–21, Jun. 2019.
- [22] H. J. Qi and M. C. Boyce, "Stress-strain behavior of thermoplastic polyurethanes," *Mech. Mater.*, vol. 37, no. 8, pp. 817–839, Aug. 2005.
- [23] D. Chiaradia, L. Tiseni, and A. Frisoli, "Compact series visco-elastic joint (SVEJ) for smooth torque control," *IEEE Trans. Haptics*, vol. 13, no. 1, pp. 226–232, Jan.–Mar. 2020.